Biomaterials 32 (2011) 8892–8904

Contents lists available at SciVerse ScienceDirect

Biomaterials

journal homepage: www.elsevier.com/locate/biomaterials

Characterization of the effects of x-ray irradiation on the hierarchical structure and mechanical properties of human cortical bone

Holly D. Barth [a,b,c], Elizabeth A. Zimmermann [a,c], Eric Schaible [b], Simon Y. Tang [d], Tamara Alliston [d], Robert O. Ritchie [a,c,*]

[a] Materials Sciences Division, Lawrence Berkeley National Laboratory, Berkeley, CA, USA
[b] Experimental Systems Group, Lawrence Berkeley National Laboratory, Berkeley, CA, USA
[c] Department of Materials Science & Engineering, University of California, Berkeley, CA, USA
[d] Department of Orthopaedic Surgery, University of California, San Francisco, CA, USA

ARTICLE INFO

Article history:
Received 22 July 2011
Accepted 7 August 2011
Available online 31 August 2011

Keywords:
Human cortical bone
Deformation
Toughness
X-ray diffraction
Tomography
Collagen

ABSTRACT

Bone comprises a complex structure of primarily collagen, hydroxyapatite and water, where each hierarchical structural level contributes to its strength, ductility and toughness. These properties, however, are degraded by irradiation, arising from medical therapy or bone-allograft sterilization. We provide here a mechanistic framework for how irradiation affects the nature and properties of human cortical bone over a range of characteristic (nano to macro) length-scales, following x-ray exposures up to 630 kGy. Macroscopically, bone strength, ductility and fracture resistance are seen to be progressively degraded with increasing irradiation levels. At the micron-scale, fracture properties, evaluated using *insitu* scanning electron microscopy and synchrotron x-ray computed micro-tomography, provide mechanistic information on how cracks interact with the bone-matrix structure. At sub-micron scales, strength properties are evaluated with *insitu* tensile tests in the synchrotron using small-/wide-angle x-ray scattering/diffraction, where strains are simultaneously measured in the macroscopic tissue, collagen fibrils and mineral. Compared to healthy bone, results show that the fibrillar strain is decreased by ~40% following 70 kGy exposures, consistent with significant stiffening and degradation of the collagen. We attribute the irradiation-induced deterioration in mechanical properties to mechanisms at multiple length-scales, including changes in crack paths at micron-scales, loss of plasticity from suppressed fibrillar sliding at sub-micron scales, and the loss and damage of collagen at the nano-scales, the latter being assessed using Raman and Fourier Transform Infrared spectroscopy and a fluorometric assay.

Published by Elsevier Ltd.

1. Introduction

Bone is a natural composite of organic, mineral and water assembled in the form of a complex hierarchical structure [1]. At the molecular level, it comprises a network of polymetric proteins, primarily type I collagen, with hard and stiff mineral nanoparticles of hydroxyapatite that reinforce it. At sub-micron levels, the collagen forms fibrils (~100 nm diameter) with mineral platelets assembled and periodically spaced on the inside and on the fibril surface; at the micron-scale such fibrils are twisted together to form collagen fibers. At even coarser scales on the order of 10 to 100 s μm, human bone's characteristic structure consists of osteons, which are concentric layers of lamellar bone, ~100 μm in diameter, that contain a central, longitudinal, tubular cavity (Haversian canal), blood vessels, and nerves, and which represent a functional unit by which the physical and biological homeostasis of bone is actively maintained.

The stiffness, strength and toughness properties[1] of bone develop from this multi-scaled, hierarchical structure [1–4], which spans from nanometer to macroscopic dimensions (Fig. 1) [5,6]; indeed, these mechanical properties are derived from very different length-scales. This is especially true with respect to resistance to fracture where a suite of physical toughening mechanisms are activated at varying length-scales. Specifically, bone derives its toughness and hence its ability to resist fracture from both intrinsic

* Corresponding author. Department of Materials Science and Engineering, University of California, Berkeley, CA, USA. Tel.: +1 510 486 5798; fax: +1 510 643 5792.
E-mail address: ROritchie@lbl.gov (R.O. Ritchie).

[1] Stiffness is related to the elastic modulus and defines the force required to produce corresponding elastic deformation. Strength, defined by the yield stress at the onset of permanent deformation or maximum strength at the peak load before fracture, is a measure of the force/unit area that the bone can withstand. The fracture toughness measures the resistance to fracture of a material.

0142-9612/$ – see front matter Published by Elsevier Ltd.
doi:10.1016/j.biomaterials.2011.08.013

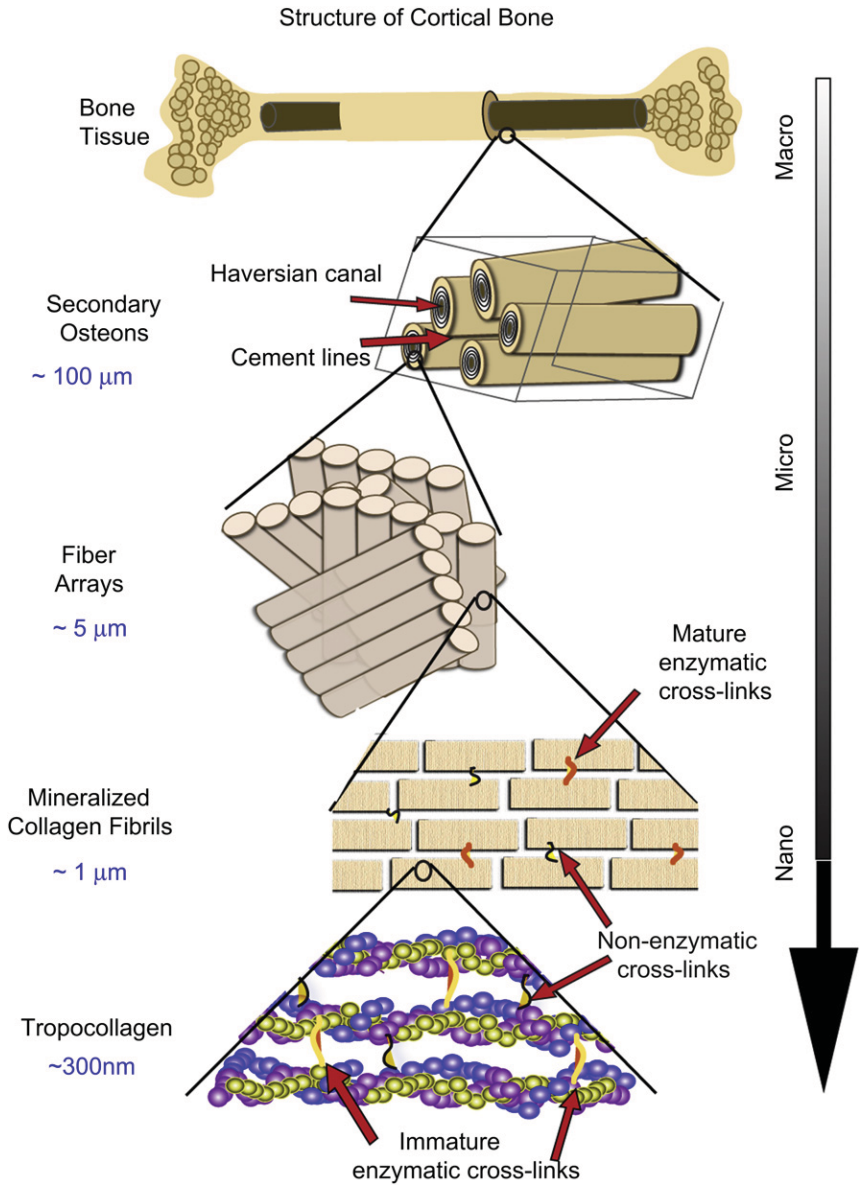

Fig. 1. The structural hierarchy of bone. At the smallest level, at the scale of the tropocollagen molecules and mineralized collagen fibrils, (intrinsic) toughening is achieved through plasticity, principally via mechanisms of molecular uncoiling and intermolecular sliding of molecules and mineralized collagen fibrils. Cross-links form at these length-scales between the collagen molecules and between the fibrils [40]. At micrometer dimensions, the breaking of sacrificial bonds at the interfaces of fibril arrays contributes to increased energy dissipation, together with crack bridging of microcracks by collagen fibrils. At the largest length-scales in the range of 10 s to 100 s μm, the primary sources of toughening are extrinsic and result from extensive crack deflection and crack bridging/twisting by uncracked ligaments, both mechanisms that are motivated by the occurrence of microcracking [5,6].

and extrinsic mechanisms (Fig. 1).[2] Principally at sub-micron dimensions, bone is toughened intrinsically by "plasticity" (or more correctly, inelasticity) mechanisms; these include the molecular uncoiling of the tropocollagen molecules at the nano-scale [6], and at slightly coarser scales the sliding of mineralized collagen fibrils [9,10]. At the length-scales of 10–100's μm, conversely, the primary toughening mechanisms in bone are extrinsic. These mechanisms affect solely the growth of cracks; they involve processes of crack-tip shielding, most notably in bone by crack deflection and twisting and bridging of the crack by fibrils or intact regions of bone-matrix in the crack wake, processes that are motivated by the presence of microcracks. A central feature for extrinsic toughening is the specific nature of the crack path which is controlled by the direction of the applied forces and the nature of the microstructure, in particular the hyper-mineralized interfaces of the osteons (cement lines), which provide microstructurally 'weak', and hence preferred, paths for cracking. Microcracks most often form at these cement lines and are thus primarily aligned with the osteonal orientation, i.e., along the long axis of the bone, with a typical spacing of ~10–100 s μm [11–15]. Indeed, ~99% of all microcracks in bone are aligned at an angle of less than 25° with respect to the osteons [16]. It is because of the orientation dependence of the microcracking, and as well as the crack arrest and

[2] *Intrinsic* toughening mechanisms operate ahead of the crack tip to generate resistance to microstructural damage. The most prominent mechanism is that of plastic deformation which provides a means of blunting the crack tip through the formation of "plastic" zones. *Extrinsic* toughening mechanisms, conversely, operate primarily in the wake of the crack tip to inhibit cracking by "shielding" the crack from the applied driving force [6–8]. Whereas intrinsic toughening mechanisms are effective in inhibiting both the initiation and growth of cracks, extrinsic mechanisms, e.g., crack bridging, are only effective in inhibiting crack growth [6].

deflection as the crack encounters the cement lines [11,17], that the fracture properties of bone are highly anisotropic, with the toughness in the transverse orientation being far higher than in the longitudinal orientations, i.e., bone is easier to split than to break.

Such mechanical properties can be adversely affected, however, by biological factors, such as aging and disease, and through exposure to irradiation. The latter can occur in medical procedures and during scientific study. Medically, bone allografts, a commonly used bone replacement in the orthopedic reconstruction of bone, are invariably sterilized with gamma radiation to minimize the spread of disease [18]. The optimum dosage, however, is somewhat controversial as too much irradiation can cause damage to the collagen matrices [19–22]. Tissue banks typically use between 10 and 35 kGy [21] although 70 kGy is needed in order to sterilize against radiation-resistant viruses.[3] For scientific studies, bone is commonly sterilized by exposure to radiation prior to testing; additionally, experiments involving *in situ* mechanical tests performed in conjunction with x-ray micro-tomography or diffraction can lead to exposures approaching 1 MGy or more[4] [24–28]. The problem here is that scientific observations and measurements on bone exposed to such radiation doses may negate the validity of the results as the structure and properties of the bone is no longer reflective of the human condition.

Recent studies [23] have shown a higher than expected effect of prior irradiation in degrading the mechanical properties of human bone. Specifically, as little as 70 kGy of radiation resulted in the total suppression of all post-yield deformation (i.e., plasticity) and after 210 kGy of irradiation, the fracture toughness was decreased by a factor of five. The decreases in strength, ductility and toughness with irradiation were attributed to (i) changes in crack path (the extrinsic effect), and (ii) a degradation of the collagen integrity from collagen damage (the intrinsic effect). Specifically, UV Raman spectra, which are known to correlate with protein conformation because of the amide moiety in cross-linking and bonding [29], indicated large increases in the amide I peak height with increased irradiation dose [23], although due to the semi-quantitative nature of spectroscopic data, the absolute levels of the cross-link profile remain unknown.

In this study, we further examine the effects of x-ray irradiation on the mechanical properties of human cortical bone over a more complete spectrum of irradiation exposures, with focus on the so-called "safe" threshold dosage for bone allografts (~25–35 kGy). We utilize a wide spectrum of "structure and property" characterization techniques explicitly to identify the magnitude of the irradiation-induced degradation in the strength, (post-yield) ductility and toughness of human cortical bone and to discern the mechanistic role of irradiation in affecting the bone-matrix structure and properties over multiple length-scales from nanoscale to macroscopic dimensions. Specifically, in addition to nonlinear elastic fracture mechanics measurements of the macroscopic bone toughness, coupled with *in situ* environmental scanning electron microscopy (eSEM) and post-testing three-dimensional synchrotron x-ray computed micro-tomography of the microscopic crack paths, we employ small- and wide-angle x-ray scattering/diffraction (SAXS/WAXD) of *in situ* uniaxial tensile tests to examine the effectiveness of fibrillar sliding as a nanoscale deformation mechanism in bone (by measuring the strain partitioning between the mineral and collagen phases), and use deep UV Raman and Fourier Transform Infrared (FTIR) spectroscopies and a fluorometric assay to characterize the damage to the collagen fibrils.

2. Experimental methods

2.1. Material

Bone test samples were taken from the midsection of a frozen human cadaveric femoral cortical bone (male, aged 48 years old). They were machined into 40 tension specimens for strength and ductility measurements (with *in situ* SAXS/WAXD) and 49 bend specimens for fracture toughness testing (with *in situ* eSEM). All samples were kept refrigerated in Hanks' Balanced Salt Solution (HBSS) prior to irradiation and/or testing.

For bend tests, the 49 samples were divided into seven groups based on irradiation exposure: one control group (unirradiated), one group irradiated at a low dose typical of radiation therapy (50 Gy), three groups irradiated at varying doses that are typical of doses received during sterilization (25, 35, 70 kGy, respectively), and two groups irradiated at the typical dose received during one to three x-ray tomography scans (210, 630 kGy). X-ray irradiation was performed at the Advanced Light Source (ALS) synchrotron facility at the Lawrence Berkeley National Laboratory on a super-bend source. The dose rate at the ALS at the energy level of 20 keV is 110 Gy/s [23]. During irradiation, all of the samples were kept hydrated by wrapping the sample in an HBSS-soaked paper towel.

The samples for each of the seven irradiation groups were further divided into two groups for mechanical testing, three samples were used for three-point bending tests and the remaining four were used for crack resistance-curve (R-curves) measurements[5]; test methods were in general accordance with ASTM standards [30]. Bend samples were machined along the long axis of the bone into 10-mm long rectangular bars (thickness $B = 1.5–2.0$ mm, width $W = 3–4$ mm). A flaw was produced in the fracture specimens by using a low-speed diamond saw to cut an initial notch, which was then sharpened by repeatedly sliding a razor blade over it with continuous irrigation with 1-μm diamond slurry. These procedures produced single-edge-notch bend (SE(B)) samples for R-curve measurements with a consistent micro-notch root radius of ~3–5 μm. Using this technique sharp stress concentrators with initial crack length of $a \approx 1.5–2$ mm ($a/W \approx 0.5$) were produced. The notch was positioned so that the nominal crack growth was perpendicular to the long axis of the bone (transverse orientation). Prior to testing, all of the notched samples were given a final polish in a 0.05 μm diamond suspension. Both the notched (for R-curve testing) and unnotched (for strength testing) samples were soaked in ambient HBSS for ~24 h prior to testing.

The 40 samples for the *in situ* tension tests were sectioned using a low-speed saw into ~10 mm long rectangular bars ($B \sim 100–200$ μm, $W \sim 1$ mm), again parallel to the bone's long axis of the bone; the final thickness was achieved by polishing with 800-grit paper. Samples were left to dry in air for roughly 24 h before 60-grit silicon carbide paper was affixed to the ends of the samples with cyanoacrylate glue to form frictional surfaces to grip during testing. Each sample had four horizontal lines drawn on with marker to act as guides for optical tracking of the tissue strain. The samples for the *in situ* tension tests were divided into two groups: a control group (unirradiated) and a high-dose irradiation group (70 kGy).

2.2. Strength, toughness and R-curve measurements

Unnotched three-point bend tests (loading span of 7.5 mm) were performed, at a displacement rate of 10 μm/s, to generate basic constitutive data for the bone samples as a function of irradiation dosage. From the resulting stress vs. strain curves, values of the ultimate bending stress and strain were determined at the point of maximum load, the bending stiffness was calculated from the slope of the stress/strain curves, and the work-of-fracture computed from the area under these curve divided by twice the cross-sectional area of the fracture surface.

In order to capture the contributions from both intrinsic (plasticity) and extrinsic (shielding) toughening mechanisms acting in the bone, fracture toughness measurements were performed using nonlinear-elastic fracture mechanics methods, specifically involving the *J*-integral[6]; in contrast to linear-elastic methods,

[3] A Gray (Gy) is a unit of adsorbed dosage of ionizing radiation, equivalent to absorbed energy per unit mass (1 Gy≡1 J/kg).

[4] A 2-mm thick bone sample is typically irradiated with ~100 Gy/s during tomographic imaging with successive scans taking up to several hours. The final dose received during these tests can involve several MGy [23], and is far above what would be considered a 'safe' threshold for bone tissue.

[5] The crack resistance- or R-curve provides an assessment of the fracture toughness in the presence of subcritical crack growth. It involves measurements of the crack-driving force, e.g., the stress intensity *K*, strain-energy release rate *G* or *J*-integral, as a function of crack extension (Δa). The value of the driving force at $\Delta a \rightarrow 0$ provides a measure of the crack-initiation toughness whereas the slope and/or the maximum value of the R-curve can be used to characterize the crack-growth toughness.

[6] *J* is the nonlinear strain-energy release rate, i.e., the rate of change in potential energy for a unit increase in crack area in a nonlinear elastic solid. It is the nonlinear-elastic equivalent of the strain-energy release rate *G*. It characterizes the stress and displacement fields at a crack tip in such a solid, and as such can be used to define the onset of fracture there.

e.g., using the stress intensity K, these methods provide a more realistic description of the contribution to the toughness from the energy consumed in plastic deformation[7] prior to, and during, fracture [11,31,32]. $J_R(\Delta a)$ R-curves were performed on hydrated bone in mode I (tensile-opening) using SE(B) specimens with a crack-growth direction transverse to the long axis of the osteons (transverse orientation). R-curves were measured with the HBSS-saturated specimens *in situ* in a Hitachi S-4300SE/N eSEM (Hitachi America, Pleasanton, CA) using a Gatan Microtest 2-kN bending stage (Gatan, Abington, UK). Crack extension was monitored directly in back-scattered electron mode at a pressure of 35 Pa and a 25 kV excitation voltage. The test method involved three-point bending with a loading span of 6 mm, with procedures conforming to ASTM Standard E1820-08 [30]. R-curve tests were terminated after approximately 700 μm of crack extension, such that measured R-curve data were limited to small-scale bridging conditions, where the size of the zone of crack bridges behind the crack tip remained small compared to the in-plane test specimen dimensions. Samples that had not failed at this stage were stored for subsequent tomography analysis.

Although nonlinear elastic J-integral measurements were made to define the driving force for crack initiation and growth, data are presented in terms of the more familiar stress-intensity factor K using the following procedures. The equivalent K value at each measured crack length was computed from the measured J values, which were determined from the applied load and instantaneous crack length according to ASTM standards [30]. Specifically, the J value was decomposed into its elastic and plastic contributions:

$$J = J_{el} + J_{pl}. \tag{1}$$

The elastic contribution J_{el} was determined from linear-elastic fracture mechanics:

$$J_{el} = \frac{K_I^2}{E}, \tag{2}$$

where K_I is the mode I stress-intensity factor, and E is Young's modulus. Using the load-line displacements, the plastic component J_{pl} for a stationary crack in bending is given by:

$$J_{pl} = \frac{1.9A_{pl}}{Bb}, \tag{3}$$

where A_{pl} is the plastic area under force vs. displacement curve, b is the uncracked specimen width (W-a). K-based fracture toughness K_{Jc} values were then back-calculated from the J measurements using the standard J–K equivalence for nominally mode I fracture, specifically that $K_{Jc} = (J_c\, E)^{½}$.

Values of the Young's modulus E for the unirradiated and irradiated (70 kGy) cortical bone were determined using nano-indentation. A total of 11 indentations were performed using a Triboindenter (Hysitron, Inc.). At each location the reduced modulus, (indicating the elastic properties of the bone extracellular matrix), was determined. The results showed a true elastic modulus of 17 ± 5 GPa with no statistically significant changes between the unirradiated and irradiated groups.

For all fracture toughness tests conducted, conditions for J-dominance, as specified by the active ASTM standard [30], were met, i.e., b, $B >> 10\,(J_c/\sigma_y)$, where σ_y is the flow stress. This latter criterion ensures that the critical J_c (and calculated K_{Jc}) values represent valid fracture toughness values.

2.3. Microstructural characterization

In addition to characterizing the bone-matrix microstructure and crack trajectories *in situ* with scanning electron microscopy (back-scattered electron mode) in the Hitachi S-4300SE/N eSEM, synchrotron x-ray computed micro-tomography (μXCT) was employed to visualize the crack path and distribution of micro-damage in three-dimensions (after R-curve testing). The μXCT evaluation was performed at the Advanced Light Source synchrotron radiation facility (Lawrence Berkeley National Laboratory, Berkeley, USA) with a setup similar to standard tomography procedures [33] in that samples are rotated in a monochromatic x-ray beam and the transmitted x-rays are imaged via a scintillator, magnifying lens and a digital camera to give an effective voxel size in the reconstructed three-dimensional image of 1.8 μm. Hydrated samples were scanned in absorption mode and the reconstructed images were obtained using a filtered back-projection algorithm. In absorption mode, the gray scale values of the reconstructed image are representative of the absorption coefficient. To maximize the signal-to-noise ratio, 20 keV energy was selected to optimize the interaction between the x-rays and the sample. Two–dimensional images were taken every quarter of a degree between 0 and 180°. The data sets were then reconstructed using the software Octopus [34] and the three-dimensional visualization was performed using Avizo™ software [35].

[7] Plastic deformation here is used as a general term to indicate any of the inelastic, non-recoverable deformation mechanisms, such as local collagen fibrillar shearing, viscoplasticity, and microcracking, that are active at various length-scales in bone [5,6].

2.4. Synchrotron x-ray scattering and diffraction measurements (partitioning of strain)

Strength and ductility measurements were also made using uniaxial tension tests under conditions where simultaneous small-angle x-ray scattering (SAXS) and wide angle x-ray diffraction (WAXD) patterns could be taken in real time. For a given strain on the bone tissue, this enabled estimates of the individual strain carried by the collagen and mineral phases. Samples were mounted in a load frame at the Advanced Light Source synchrotron facility (Lawrence Berkeley National Laboratory, Berkeley, CA) so that the long axis of the bone was oriented perpendicular to the 10 keV x-rays; a schematic of the experimental setup is shown in Fig. 2. A tensile load was applied parallel to the long axis of the femur. The sample was kept hydrated 12 h prior to the experiment as well as throughout the experiment by means of a hydration cell comprised of a strip of cellophane held to the sample through capillary action with a few drops of HBSS.

A parallel beam of monochromatic x-rays (at an energy of 10 keV and a wavelength of 0.124 nm) with a 1 mm × 0.25 mm cross-section was directed perpendicular to the applied load. A high speed Pilatus detector was used for collecting SAXS data and a Quantum CCD X-ray detector (Area Detector Systems Corporation) was used for reading WAXD patterns. The sample was mounted into a custom built tensile stage fitted with a 5-kgf load cell (Omega, LC703-10) and a motor-driven displacement stage. All samples were loaded under displacement control at a displacement rate of 1 μm/s, with SAXS/WAXD measurements taken at various points along the stress/strain curves, with an exposure time for the frames of 0.5 s. The number of exposures was regulated in order to keep the radiation dose below 30 kGy so that there would not be any additional damage to the tissue due to the radiation received during *in situ* tensile testing; specifically, the x-ray irradiation was blocked between exposures.

Synchrotron radiation was used to measure the SAXS and WAXD patterns which were analyzed to find percent changes in the fibril and mineral strain along the tensile axis. For the SAXS region of reciprocal space, the meridional collagen molecules in the fibril have a staggered spacing of ~67 nm (this leads to a diffraction peak at a q-value of ~0.009 $Å^{-1}$), where the mineral is primarily deposited between the heads and tails of the collagen, leading to a diffraction pattern. The SAXS detector was located at a distance of ~4100 mm from the sample in order to detect changes to the collagen peak position. The WAXD detector was placed ~250 mm away from the sample. For the WAXD region of reciprocal space the detector must be oriented to get diffraction from the (0002) peak at a lattice spacing of ~0.344 nm. The sample-detector distance and the beam center were both calibrated for the SAXS/WAXD data analysis using a silver behenate standard. The analysis software IGORPro (Wavemetrics) and the custom macro NIKA were then used in conjunction to convert the 2-D data to 1-D by radially integrating the 2-D SAXS and WAXD patterns over azimuthal sectors. For this experiment SAXS/WAXD patterns were integrated in a narrow pie shaped sector with a 10° angular width that was centered along the tensile axis. After integration the peaks representing the first order reflection from the meridional collagen SAXS pattern and around the (0002) reflection from the apatite WAXD pattern were fit using a Gaussian function and a fourth order polynomial. The peak positions were used to find, respectively, the collagen fibril D-spacing and the (0002) crystallographic lattice spacing relative to the unstressed state (defined at zero load for each sample).

The tissue strain was measured by measuring percent changes in the distance between the two horizontal lines on either end of the samples using image analysis software (National Instruments Vision Assistant 8.5). This was achieved using a CCD camera synchronized with the detectors to take images when the samples were exposed to x-rays during testing.

2.5. Fourier transform infrared spectroscopy

Fourier transform infrared (FTIR) spectroscopy was used in transmission mode to assess the degree of enzymatic cross-linking in the collagen for two groups: healthy (unirradiated) and irradiated (70 kGy) human cortical bone. Ten samples of human cortical bone were sectioned with a low-speed saw. The tissue was dehydrated with a series of ethanol baths to remove the water component, which has a strong absorbance in the IR spectrum. The samples were then embedded in Technovit 7100 (Kultzer & Co, Wehrheim, Germany), a liquid containing hydroxyethyl-methacrylate, according to the manufacturer's instructions. Briefly, Technovit 7100 was admixed with hardener I and II at 300:3:20 v/w/v ratio, as described in [36]. The embedded tissue was then sectioned with a microtome to a final dimension of ~1 mm × 1 mm × 2 μm as a 1–5 μm thickness is required to analyze the samples with IR beam in transmission.

The protein Amide I (peptide bond C=O stretch) undergoes frequency and intensity changes as a result of changes in protein secondary structure [37]. One of the unique capabilities of FTIR spectroscopy is the ability to quantify these changes, specifically by tracking the spatial variation of the collagen components in mineralized tissue. Information on the protein structure can be extracted from broad spectral bands consisting of components of peaks resulting from Amide I modes of various secondary structures by using a spectral resolution technique [38]. For type I collagen in bone the two major components of importance are the enzymatic collagen cross-links: pyridinoline (Pyr) and divalent dehydrodihydroxynorleucine

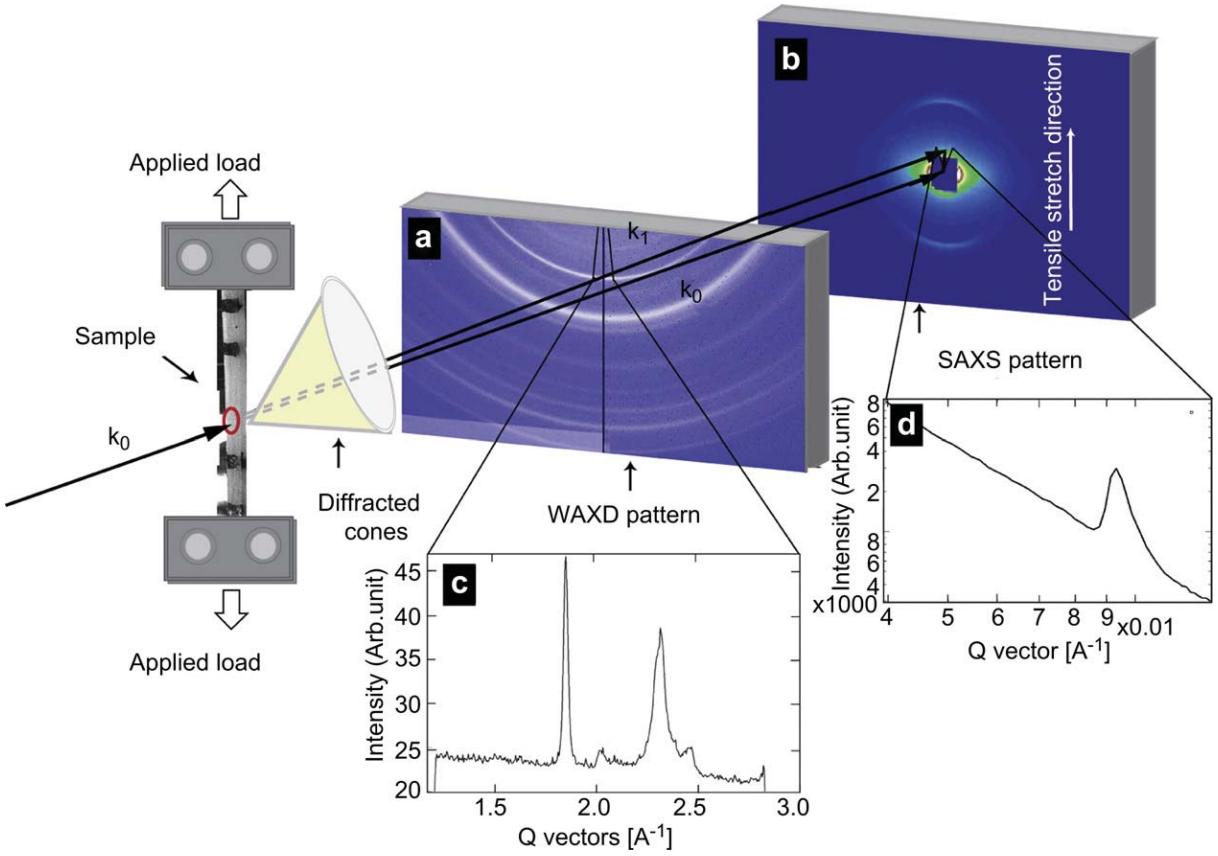

Fig. 2. Schematic showing the beamline setup for *in situ* tensile testing of bone with real time small-angle x-ray scattering and wide-angle x-ray diffraction (SAXS/WAXD) imaging. The 10 keV x-ray beam penetrates the longitudinally oriented human cortical bone sample perpendicular to the tensile set up. The SAXS detector is positioned to record the meridional *D*-spacing in the staggered array of mineralized collagen fibrils. The WAXD detector is positioned to record patterns from the crystallites with *c*-axis along the tensile direction. Tissue strain is determined by the marker lines on the sample (camera not shown in schematic). Images (a) and (b) show WAXD pattern and the SAXS pattern of bone respectively, with the region for azimuthal integration shown in the pie-shaped sector outlined in both. Figures (c) and (d) show the integrated intensity variation over this region. Graph (c) shows a pronounced (0002) diffraction peak for the hydroxyapatite, and graph (d) shows a pronounced first order diffraction peak due to the fibrillar *D*-spacing (67 nm).

(DHLNL). Indeed, the ratio of peak areas of the Pyr and DHLNL subbands, at 1660 cm^{-1} and 1690 cm^{-1} respectively, provides a semi-quantitative measure of the cross-linking profile in the collagen matrix; this ratio has been correlated to the relative amounts of enzymatic cross-links, specifically mature non-reducible (interfibrillar) cross-links and immature reducible (intrafibrillar) cross-links (Fig. 1). A method has been developed to enable spectral analysis of the amide I band to isolate peaks corresponding to these two major type I collagen cross-links, namely pyridinoline (pyr) and DHLNL [39], using second-derivative spectroscopy. All FTIR spectroscopy data were obtained using a conventional Globar IR source at the Advanced Light Source (Lawrence Berkeley National Laboratory, Berkeley, USA). Image spectroscopy consists of a source, a sample handling unit and a focal plane array detector on an IR microscope. The instrument is equipped with a photographic device to capture an image of the area of the tissue being examined. The recorded spectra were taken in transmission mode with 128 scans and had a spectral resolution of 4 cm^{-1} and a spot size of ~150 μm. OMNIC software (Thermo Fischer) was used for data processing.

2.6. Deep ultraviolet Raman spectroscopy

The collagen cross-linking profile was further characterized using deep-ultraviolet Raman spectroscopy, with a 244-nm excitation source [23]. The UV Raman technique eliminates the fluorescence interference found with visible excitation. Also, due to resonance effects, the signal strength of some features from the organic phase (particularly those associated with the amide moiety formed by the bonds between peptides) are enhanced relative to those from the inorganic phase (e.g., phosphate and carbonate stretching modes). To avoid damage to the sample the laser power was kept below 5 mW and the sample was rotated at ~45 rpm. It is known [23,29] that the height of the amide I feature at 1650 cm^{-1} is sensitive to the collagen environment, in particular to the extent of cross-linking, increasing, for example, with dehydration or with increasing tissue age. For quantitative analysis of this effect, spectra were processed by subtracting a small linear background defined by the signal at 500 and 2000 cm^{-1} and then normalizing to the height of the CH_2 wag peak at 1460 cm^{-1} (this peak does not have a strong resonance enhancement).

2.7. Accumulation of advanced glycation end-products

Bone collagen is also susceptible to the age-related accumulation of non-enzymatic cross-links resulting from the covalent bonding of oxidizing sugars and free amino groups on the collagen protein including arginine and lysine. These cross-links are known as advanced glycation end-products (AGEs) and they form both intra- and inter- fibrillar links along the collagen backbone [40]. The AGEs were quantified using a fluorometric assay on both unirradiated bone and bone irradiated at 70 kGy. For each sample a section of the femoral midshaft was demineralized using ethylenediaminetetraacetic acid (EDTA) and then hydrolyzed using 6N HCl for 24 h at 110 °C. AGE content was determined using fluorescence readings taken using a microplate reader at the excitation wavelength of 370 nm and emission wavelength of 440 nm. These readings were standardized to a quinine-sulfate standard and then normalized to the amount of collagen present in each bone sample. The amount of collagen for each sample was determined based on the amount of hydroxyproline, the latter being determined using a chloramine-T colorimetric assay that recorded the absorbance of the hydrolysates against a commercially available hydroxyproline standard at the wavelength of 585 nm [41].

3. Results

3.1. Strength, ductility and fracture toughness

Bending stress-strain curves, which assess the macroscopic strength and ductility, and fracture toughness R-curves of human cortical bone irradiated at varying degrees of x-ray irradiation (0, 0.05, 25, 35, 70, 210, 630 kGy), are shown in Fig. 3. Data show that for irradiation exposures starting between 35 and 70 kGy, there is a severe dose-dependent degradation in mechanical properties; no effect could be discerned at 35 kGy and below. Above this level though, there was a complete loss in post-yield deformation

(plasticity) coupled with a progressive and very severe reduction in the ultimate (maximum) bending strength, bending strain and toughness, although little change was seen in the bending stiffness. Specifically, compared to unirradiated bone, exposures of 70, 210 and 630 kGy resulted in a respective decrease in the strength of the bone by ~25%, 60% and more than 80%, while a similar trend was observed for the ultimate strain (Fig. 3a), consistent with previous studies that showed that γ- and x-irradiation can degrade the plastic, rather than elastic, properties of bone, such as bending strength and toughness [22,42–47].

The corresponding toughness properties, in terms of full $K_R(\Delta a)$ R-curves for physiologically relevant small cracks ($\Delta a < 700$ μm), are plotted in Fig. 3b for all seven irradiation groups. It was observed that even though the stress-strain curves showed a severe loss in the plastic properties of bone with high doses of irradiation, rising R-curve behavior is still exhibited (albeit diminished), even after all plasticity is lost, indicating that some limited degree of extrinsic toughening, e.g., from crack deflection and/or crack bridging, is still active. Nevertheless, the irradiation caused a very severe degradation in the crack-initiation toughness (assessed in terms of the intercept of the R-curve at $\Delta a \rightarrow 0$) and crack-growth toughness (assessed as both the slope of the R-curve, $dK/d\Delta a$ and the instability toughness value, K_{Jc}). Specifically, over the first 600 μm of (subcritical) crack extension, K_{Jc} fracture toughness values were as much as a factor of five lower after 210 kGy irradiation, i.e., from values of 13.3 MPa√m ($J_c \sim 9$ kJ/m^2) in unirradiated samples down to 2.7 MPa√m ($J_c \sim 0.3$ kJ/m^2) in the 210 kGy irradiated samples; similarly, K_{Jc} values were 10.5 MPa√m ($J_c \sim 5$ kJ/m^2) and 7.4 MPa√m ($J_c \sim 3$ kJ/m^2), respectively, after 50 Gy and 70 kGy of radiation.

3.2. Crack path observations

The nature of the crack trajectories in relation to the microstructure is illustrated in Fig. 4 for human cortical bone subjected to (a-c) low dose (50 Gy) and (e-f) high dose (~MGy) x-ray irradiation as two-dimensional x-ray tomographic images (a,c) and (d,f) and three-dimensional representations (b) and (e) of the crack path and Haversian canals. Specifically, Fig. 4a–c show how the growing crack is severely deflected and twisted as it encounters the osteons in low dose irradiated bone, with the result that the crack path is highly deflected in all orientations. Such characteristic features of extrinsic toughening are typical of unirradiated bone [11,48], and are consistent with the notion that irradiation exposures of 50 Gy do not appear to significantly harm the toughness properties of the bone. In stark contrast, the crack trajectories in the severely irradiated bone, shown in Fig. 4d–f, are quite different, with far less evidence of major crack deflections at the osteon boundaries and a resulting relatively planar crack path. The mechanisms of crack deflection and twist are still operative, but their limited size leads to much smaller amplitude deviations in crack path and hence to lower toughness, consistent with the macroscale test data in Fig. 3.

3.3. SAXS/WAXD for tissue strain measurements

To further investigate the loss in plasticity with irradiation, hydrated bone samples were loaded in uniaxial tension with simultaneous examination using SAXS/WAXD. For a given strain in the bone tissue sample, the individual strains in the collagen and mineral were measured in human cortical bone exposed to 70 kGy of x-ray irradiation, as compared to unirradiated bone. Results are shown in Fig. 5a,b, respectively, for the variation in individual strains in the collagen fibrils (ε_F) and in the mineral (ε_M), as a function of the global strain (ε_T) applied to the bone tissue. With increasing tissue strain, a linear increase in both the fibrillar and mineral strain is apparent, until yielding occurs at roughly 1% tissue strain (Fig. 6); at this point most of the strain continues to be carried by the collagen, but not in the irradiated bone, which then fractures. With plastic deformation, the fibrillar and mineral strains assume approximately constant values (~1.1% in the collagen, ~0.2% in the mineral), consistent with results in the literature [10]. Following 70 kGy irradiation, however, the fibrillar strains are roughly up to 50% lower for a given tissue strain, and the sample fails catastrophically with little to no evidence of post-yield deformation, indicative of the loss of plasticity in highly irradiated bone. The actual ratios of fibrillar to tissue strain ($\varepsilon_F/\varepsilon_T$) and mineral to tissue strain ($\varepsilon_M/\varepsilon_T$) are plotted for both groups in Fig. 6 to compensate for sample-to-sample variability. The strain carried by the collagen fibrils in the 70 kGy irradiated samples is ~40% of the applied tissue strain, which is considerably lower than in the unirradiated bone where the fibril strain is ~80% of the tissue strain. The effect is summarized in Fig. 7 where at an applied tissue strain of 0.85%, exposure to 70 kGy of irradiation causes a ~40% decrease in the strain carried by the collagen fibrils and a ~20% decrease in mineral strain, as compared to unirradiated bone. The data for the tissue and mineral strain are both binned in regular

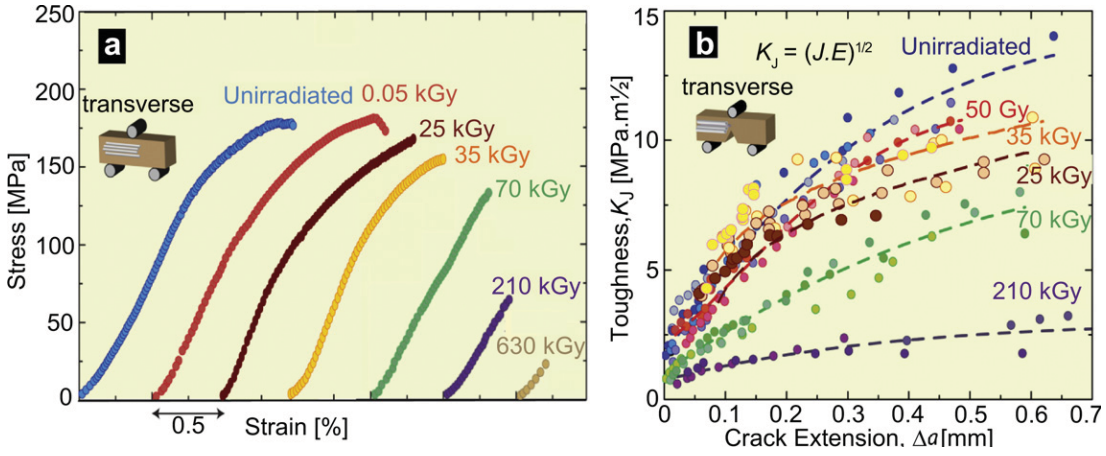

Fig. 3. Mechanical properties of hydrated human cortical bone (transverse orientation) subjected to varying degrees of x-ray irradiation. (a) Stress-strain curves from three-point bending tests (offset for clarity) and (b) fracture toughness R-curves showing resistance to fracture in terms of the stress intensity, K_J, as a function of crack extension, Δa, both as a function of prior x-irradiation dosage. K_J fracture toughness values were back-calculated from J measurements using the J-K equivalence for mode I fracture. The end of the curves indicates the critical toughness values, K_{Jc}, at which complete failure occurred.

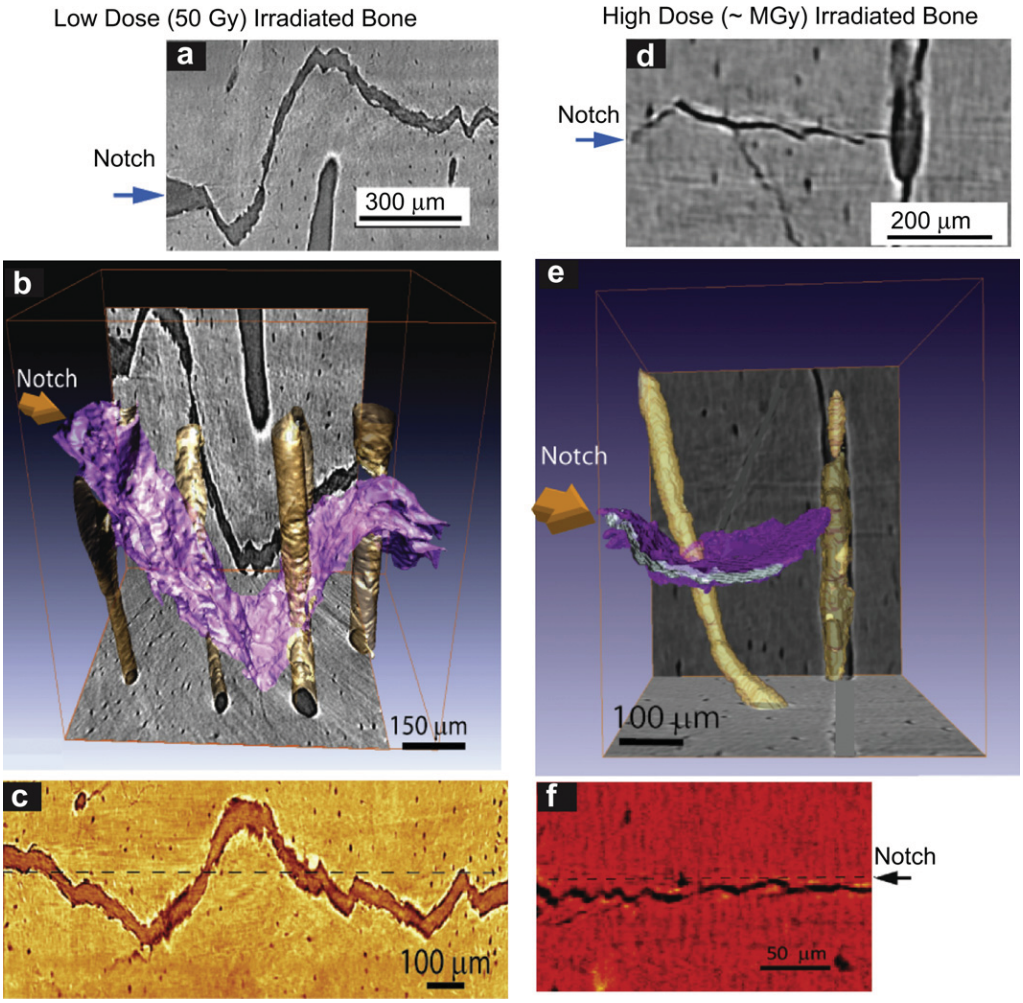

Fig. 4. X-ray computed micro-tomography of crack paths in hydrated human cortical bone in the transverse orientation following (a–c) low dose (50 Gy), and (e–g) high dose (~MGy) x-irradiation. Images show crack paths: (a) & (d) x-ray tomographs from side-view perpendicular to the crack plane, (b) & (e) 3-D x-ray tomography images of these paths (3-D crack surface is in purple; Haversian canals are yellow), and (c) & (f) 2-D tomographs of the paths from the back face of the sample. The crack deflects on encountering the osteons; such crack deflection and crack twisting is the prime extrinsic toughening mechanism in bone in the transverse orientation. Note, however, that the frequency of such deflections increases with irradiation while their severity decreases, resulting in less meandering crack paths in the irradiated bone. (For interpretation of the references to colour in this figure legend, the reader is referred to the web version of this article.)

intervals of tissue strain ($N = 20$ for each group), with error bars representing the standard errors of mean.

3.4. Quantification of collagen cross-linking

As high doses of irradiation are known to impart severe damage to the collagen matrix in the form of breaking of peptide bonds in the collagen backbone [21,23,49], the nature of the collagen environments was examined specifically using a number of techniques.

As we reported previously [23], results from deep UV-Raman spectra, shown in Fig. 8 for (hydrated) unirradiated and all irradiated groups of bone, indicate a very pronounced increase in the amide I peak after exposure to x-rays, implying severe damage of the collagen with increasing degree of irradiation. Although this indicates significant changes in the collagen environment associated with increased cross-linking, the identification of the specific nature of the cross-links with this technique remains uncertain.

For this reason, in the present study we performed additional Fourier transform infrared (FTIR) spectroscopy on unirradiated and 70 kGy irradiated bone. The protein amide I (peptide bond C=O stretch) mode near 1650 cm^{-1} undergoes frequency and intensity changes as a result of changes in protein secondary structure. FTIR spectroscopy gives quantitative information on the collagen maturity in bone, specifically the ratio of two of the major enzymatic collagen cross-links: namely, the mature (non-reducible) divalent cross-links (Pyr) and the enzymatic immature (reducible) divalent dehydrodihydroxynorleucine cross-links (deH-DHLNL). Of these components the relative percent area ratio of the two sub-bands at ~1660 cm^{-1} and ~1690 cm^{-1} is related to collagen cross links that are abundant in mineralized tissue (Pyr and deH-DHLNL, respectively) [39]. For our results (Fig. 9), a comparison of the calculated 1660:1690 spectroscopic ratio of these two peaks in the two groups of bone is shown in Fig. 9a. The ratios are calculated using second derivative spectroscopy which locates the position of the underlying bands within the amide I region and then peak fits these sub-bands to obtain information on the relative percent area contribution of each underlying component for the unirradiated and 70 kGy irradiated groups. The 1660:1690 peak area ratio appears to correspond to the ratio of non-reducible (mature) to reducible (immature) collagen cross-links in bone [39]. The results show that following 70 kGy irradiation, the 1660:1690 ratio decreases by almost two-thirds, indicating that the damaging effects of irradiation affect the mature cross-links such as Pyr to a greater degree than the immature cross-links such as deH-DHLNL.

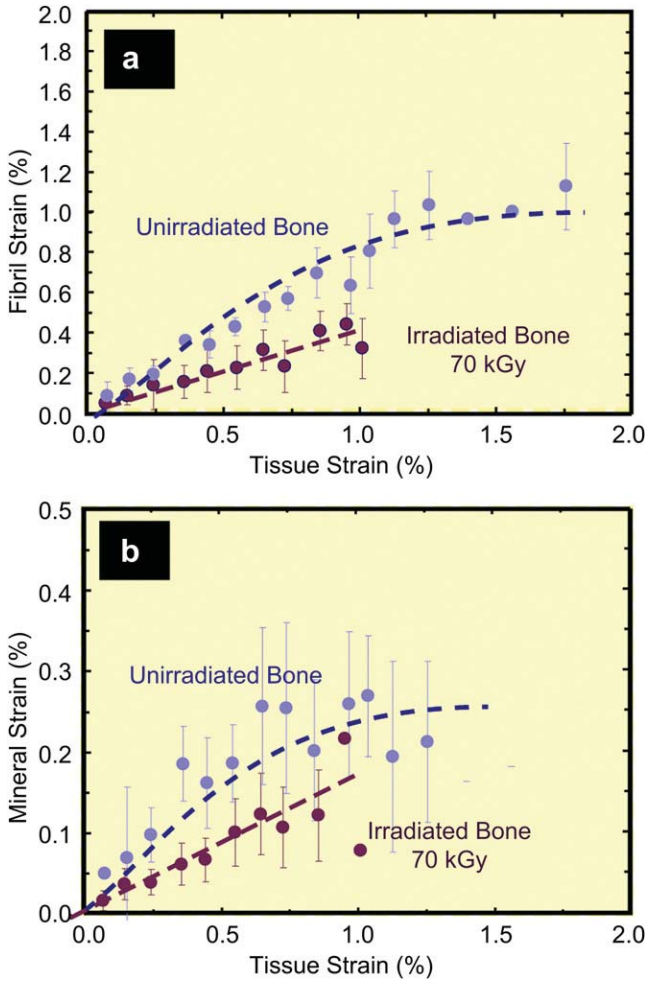

Fig. 5. Partitioning of strain between the collagen and mineral as a function of the global tissue strain in 70 kGy irradiated vs. unirradiated hydrated human cortical bone. Variation of the strain from SAXS/WAXD measurements in the (a) collagen and (b) mineral as a function of the global applied strain in the bone tissue for unirradiated and 70 kGy irradiated bone. The collagen and mineral strain are binned in regular intervals of tissue strain ($N = 20$ for each group). Error bars in the graphs are standard deviation of the binned value. Note that for a given strain in the bone tissue the strain in the collagen fibrils is diminished in irradiated vs. unirradiated bone, consistent with the progressive loss in macroscopic plasticity in bone with increasing irradiation.

The quantification of non-enzymatic cross-links was achieved via a fluorometric assay that determines the relative intrinsic fluorescence due to advanced glycation end-products (AGEs) relative to the amount of collagen in the bone-matrix. We find that bone which has been exposed to 70 kGy irradiation has an elevated concentration of AGEs, on the order of ~21%, as compared to that in unirradiated bone (Fig. 10).

4. Discussion

Although irradiation is known to deleteriously degrade the structure and mechanical properties of bone, we show in this work that the effect can be extremely severe; indeed, the tissue can be dramatically and irreversibly embrittled with major losses in strength, ductility and fracture resistance following exposures in excess of 35 kGy. Specifically, compared to healthy (unirradiated) human cortical bone, we find that bone strengths are reduced by ~60% and more than 80% for irradiation doses of 210 and 630 kGy, respectively, with a factor of five loss in fracture toughness at 210 kGy. Additionally, for x-ray irradiation exposures above ~70 kGy, the bone no longer displays evidence of post-yield ("plastic") deformation, simply failing at its elastic limit (Fig. 3).

We explain these effects in terms of how the irradiation affects the intrinsic and extrinsic contributions to the bone toughness, which are developed at widely different structural length-scales. At micro- to macro-scales, the major contributions to the fracture toughness originate extrinsically through such mechanisms as crack deflection and bridging. The key here is the occurrence of microcracking, which predominates along the "weaker" hypermineralized interfaces of the osteons (cement lines) and to a lesser extent along the lamellar boundaries. In the longitudinal orientations, (cement line) microcracks are aligned roughly parallel to the growing crack; their formation alongside and ahead of the crack tip leaves locally intact regions that can act as bridges across the crack ("uncracked-ligament" bridging), and can carry load that would otherwise be used to promote cracking [48]. The extent of toughening, however, is far larger in the transverse direction, the orientation examined in this study, as the microcracks are now aligned roughly perpendicular to the crack path where they act as "delamination barriers" [11,17]; this serves to locally arrest growing cracks, cause marked crack deflections and crack twists, generate highly tortuous crack paths, extremely rough fracture surfaces, and correspondingly high toughness (Fig. 4a–c). Specifically, the growing cracks deflect by as much as 90° as they encounter these interfaces between the interstitial bone and the osteons; the consequent marked crack deflections and through-thickness twists (Fig. 4a–c) are the primary source of (extrinsic) toughening in the transverse orientation.

Prior exposure to x-rays at dosages in excess of ~70 kGy, however, leads to radical changes in the crack path (Fig. 4d–f). Although growing cracks are still subject to such microstructurally-induced deflections, the deflections are far smaller in magnitude (although more frequent) resulting in minimal crack-path deviations and an essentially linear crack trajectory (Fig. 4d–f). It is the absence of such highly tortuous crack paths in irradiation-damaged bone, with minimal deviations from the plane of maximum tensile stress, that serves to curtail the high extrinsic toughness which is characteristic of healthy bone in the transverse orientation.

In many respects though, it is the effects of irradiation on the intrinsic contributions to the bone toughness that are more interesting. These contributions arise at much smaller (sub-micron) length-scales and are associated primarily with the generation of "plasticity" in bone from the process of fibrillar sliding, which can occur at both the fibril [10] and fiber [50] level. Within the fibrils non-recoverable deformation mechanisms take place, such as sliding at the HA/tropocollagen interface [9], increased intermolecular cross-linking density [40] and sacrificial bonding [51]; these mechanisms constrain molecular stretching and provide the basis for the increased apparent strength of the collagen molecules without catastrophic failure of either of the individual components. The molecular behavior of the protein and mineral phases (fibrillar sliding) within a fibril enables a large amount of dissipative deformation energy once plastic yielding begins in mineralized tissues [10,52,53] and other biological materials [54]. At the nanoscale the predominant plasticity mechanisms are represented by this model of load transfer. As is common in most materials, plasticity contributes to the intrinsic toughness by dissipating energy and forming "plastic zones" surrounding crack-like defects that further serve to blunt crack tips, thereby protecting the integrity of the entire structure by reducing the driving force (i.e., stress intensity) for crack propagation.

Changes to the effectiveness of this intrinsic mechanism are largely influenced by the organic matrix. In this regard, damage to the collagen matrix induced by irradiation can be extremely problematic to the biomechanical properties of bone, in particular

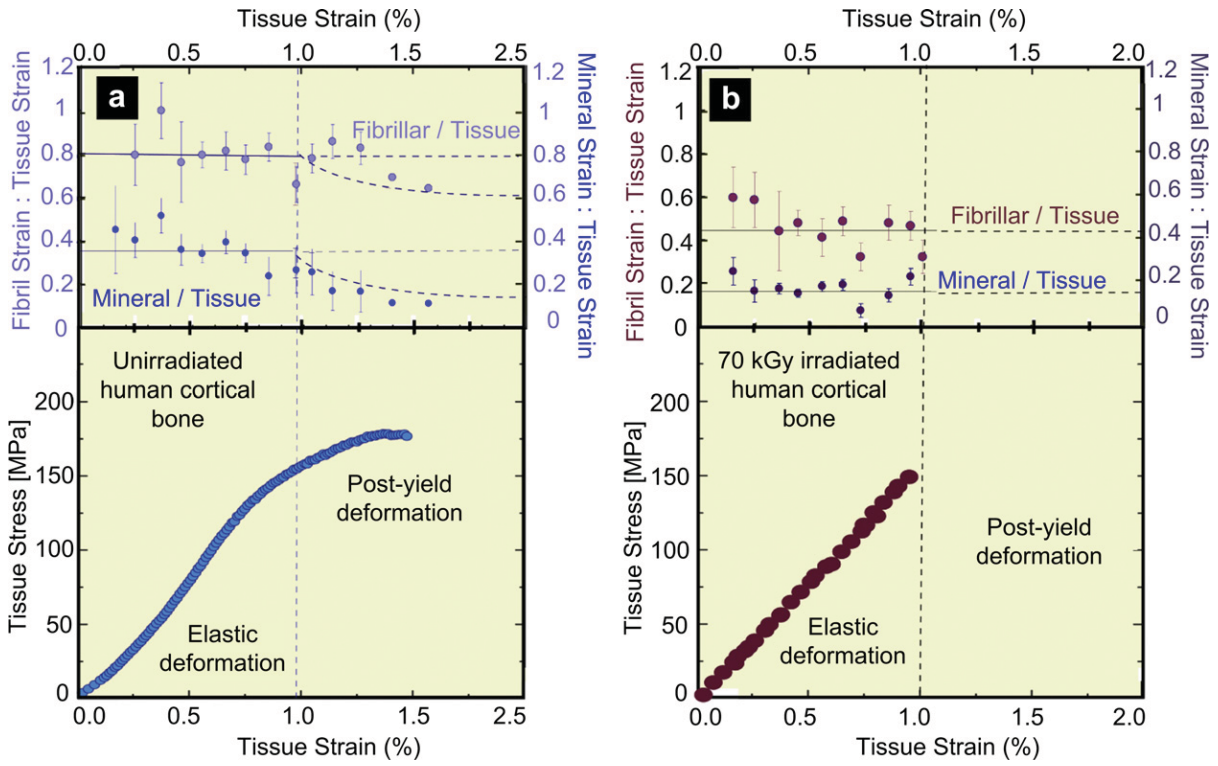

Fig. 6. Strain in collagen fibril, and mineral in bone as a function of applied strain in the tissue for human cortical bone in the (a) unirradiated and (b) 70 kGy irradiated condition. The upper graphs show the ratios of fibril to tissue strain, $\varepsilon_{F}/\varepsilon_{T}$, and mineral to tissue strain, $\varepsilon_{M}/\varepsilon_{T}$, for the (a) unirradiated and (b) 70 kGy irradiated bone, averaged from $N = 20$ samples for each group. In (a) and (b), the solid lines represent the constant strain ratio expected before yield. In (a), the dotted line represents where the ratio would vary if the fibril and mineral strain remained constant beyond the yield strain. The lower graphs show the corresponding stress-strain curves for the (a) unirradiated and (b) 70 kGy irradiated human cortical bone.

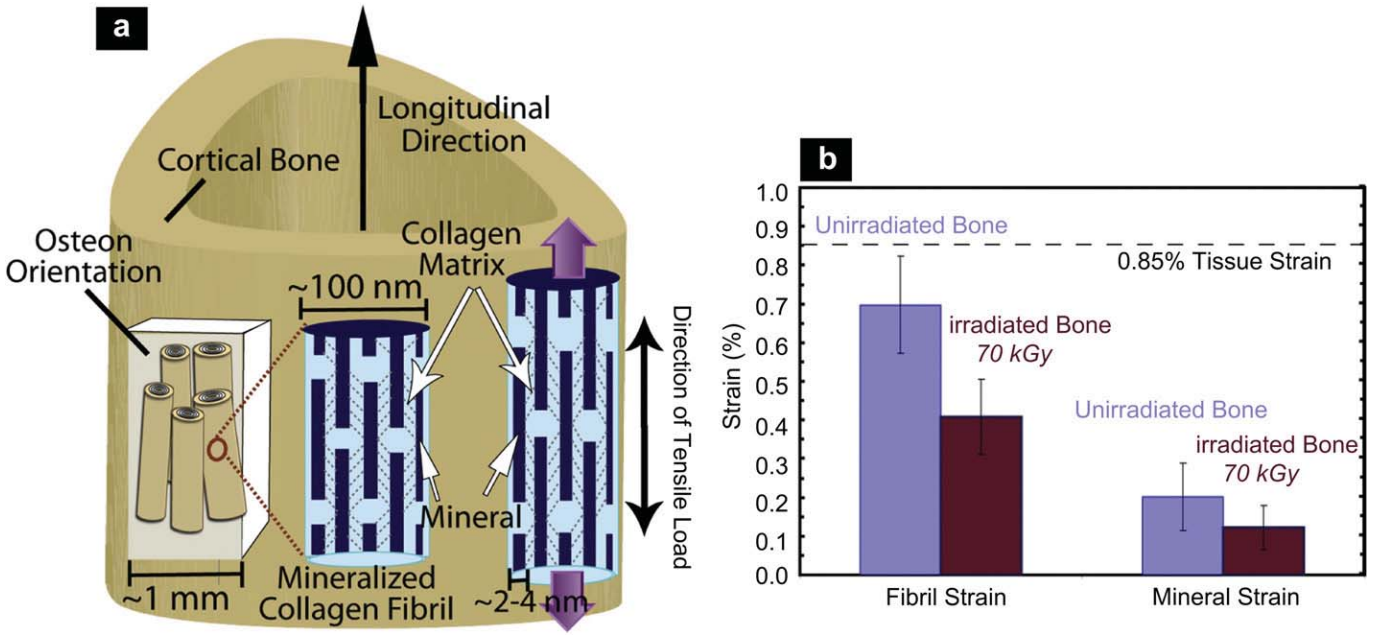

Fig. 7. (a) Schematic illustration of the sample orientation in relation to the bone-matrix microstructure in human cortical bone (top) and schematic model for bone deformation for the various hierarchical length-scales in response to external tensile load. Strain is simultaneously measured at all three levels of the structural hierarchy (tissue, fibril, and mineral nanoparticles). The mineralized fibrils, which are stiffened with collagen cross-links, deform in tension and transfer the stress between neighboring fibrils by shearing in the thin layer of the matrix. Within each mineralized fibril, the stiff mineral platelets deform in tension and transfer stresses between adjacent platelets by shearing in the interparticle collagen matrix. (Red lines demonstrate shearing qualitatively). (Adapted from ref. [10]) (b) At a fixed tissue strain of 0.85%, the individual strain in the fibrils is 42% less in the 70 kGy irradiated bone than in the healthy unirradiated bone. (For interpretation of the references to colour in this figure legend, the reader is referred to the web version of this article.)

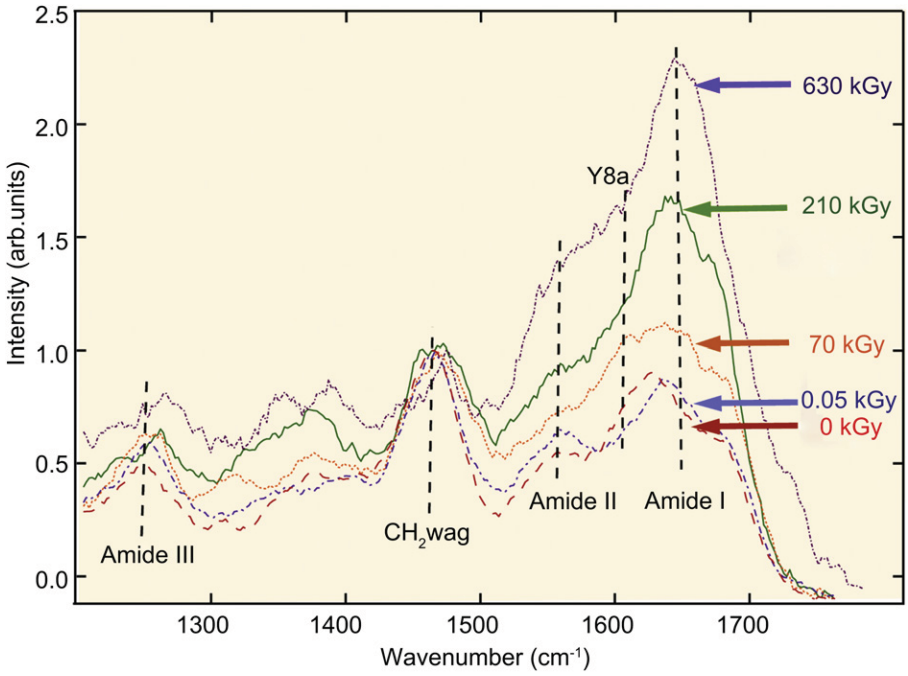

Fig. 8. UV-Raman spectroscopy of (hydrated) unirradiated and x-irradiated human cortical bone. (a) UV-Raman spectra for five different irradiation groups after doses of 0, 0.05, 70, 210 and 650 kGy, showing specifically the large changes in the relative height of the amide I feature compared to the CH_2 wag peak. The amide I (primarily from C≡O stretch) peak has previously been a good indicator for observing changes in the protein arrangement as the amide is known to play a role in cross-linking and bonding. The amide I peak height of the peak monotonically increases with irradiation, consistent with an increase in cross-linking in the collagen. Some of the other noticeable organic features for the bone-matrix are the CH_2 wag peak (1454–1461 cm^{-1}), amide III (primarily from in-phase combination of NH in-plane bend and CN stretch, 1245–1260 cm^{-1}), and amide II (primarily from out of phase combination of NH in-plane bend and CN stretch). (Additional data from ref. [23]).

through the formation of collagen cross-links [55–58] and eventually breakage of the backbone of the collagen molecule. In this regard, the profile and distribution of collagen cross-links have a major influence on bone function. As noted, three major types of collagen cross-links are found in human cortical bone: enzymatic immature (reducible) divalent cross-links (dehydrodihydroxynorleucine) and mature (non-reducible) divalent (pyridinoline and pyrrole) cross-links linking neighboring fibrils, and the non-enzymatic advanced glycation end-products (AGEs) that form both intermolecular and interfibrillar cross-links along the collagen backbone. Intermolecular cross-linking provides the fibrillar matrices with properties such as tensile strength and viscoelasticity [40,59–61]. The staggered array of type I collagen, the primary type found in bone, relays strength in tension; the cross-links keep the array in conformity - if there are too many cross-links collagen's ability to absorb energy declines, if there are too few the array may break apart. A similar effect is thought to occur at the next structural level between arrays of fibrils [50], which are linked via non-collagenous proteins and cross-linking.

In the current work, macroscopic mechanical tests clearly indicate that a primary aspect of the irradiation-induced loss in fracture resistance can be attributed to a complete loss in post-yielding (plastic) deformation (intrinsic toughness) for radiation exposures of 70 kGy and above. Based on SAXS/WAXD analyses and associated cross-link measurements, we interpret this in terms of a suppression of the prevailing plasticity mechanism in bone of fibrillar sliding, which results principally from a change in the proportion of the three types of collagen cross-linking caused by the irradiation damage.

At the onset of plastic deformation in healthy (unirradiated) bone (Figs. 5 and 6), the strain in the mineral becomes roughly constant with increasing tissue strain (Fig. 5b). Initially the load in the bone is carried by the mineral particles through shearing of the collagen matrix [62], but once yielding occurs the mineralized fibril and the fibril matrix begin to decouple [53]; a schematic interpretation for the load transfer in bone is shown in Fig. 7. The tensile strain can be divided into two contributions: first from the tensile stretching of the mineralized collagen fibrils (which we studied by examining changes in the 67 nm d-spacing) and second by shear deformation of the interfibrillar matrix and, at the smallest length-scale, by shearing of the collagen matrix through the transfer of stress between the stiff mineral platelets [10,63]. In contrast, once plastic deformation begins in the irradiated bone, the tissue fails due to degradation of the collagen matrix, which acts to totally eliminate the bone's capacity for plastic deformation; in materials science terms, the bone simply "embrittles" due to irradiation.

Our spectroscopy and fluorometric measurements (Figs. 8–10) strongly suggest that this progressive irradiation-induced embrittlement of bone in the form of the suppression of plasticity from fibrillar sliding and the consequent major losses in toughness initially result from an increase in specific collagen cross-linking which raises the amount of bonds; further irradiation exposures can cause molecular damage due to breaking the peptide backbone. Irradiation exposure leads to the release of free radicals via radiolysis of water molecules in bone which can severely degrade the collagen molecules in addition to restricting fibrillar sliding mechanisms [21,49,64].

Specifically, we observe a significant change in the magnitude of the amide I peak in UV Raman spectra with radiation indicative of a radically changed collagen environment (Fig. 8). Indeed, these measurements show that for a very large exposure of 630 kGy, the spectral features were broadened to such an extent that the individual peaks could not be observed, which is likely associated with breaking of peptide bonds in the collagen backbone [49]. Although this change in the height of the amide I peak has been related to collagen cross-linking [23,29], we obtained further information on the nature of these cross-links using FTIR spectroscopy techniques to measure the vibrational energies of molecules to detect changes

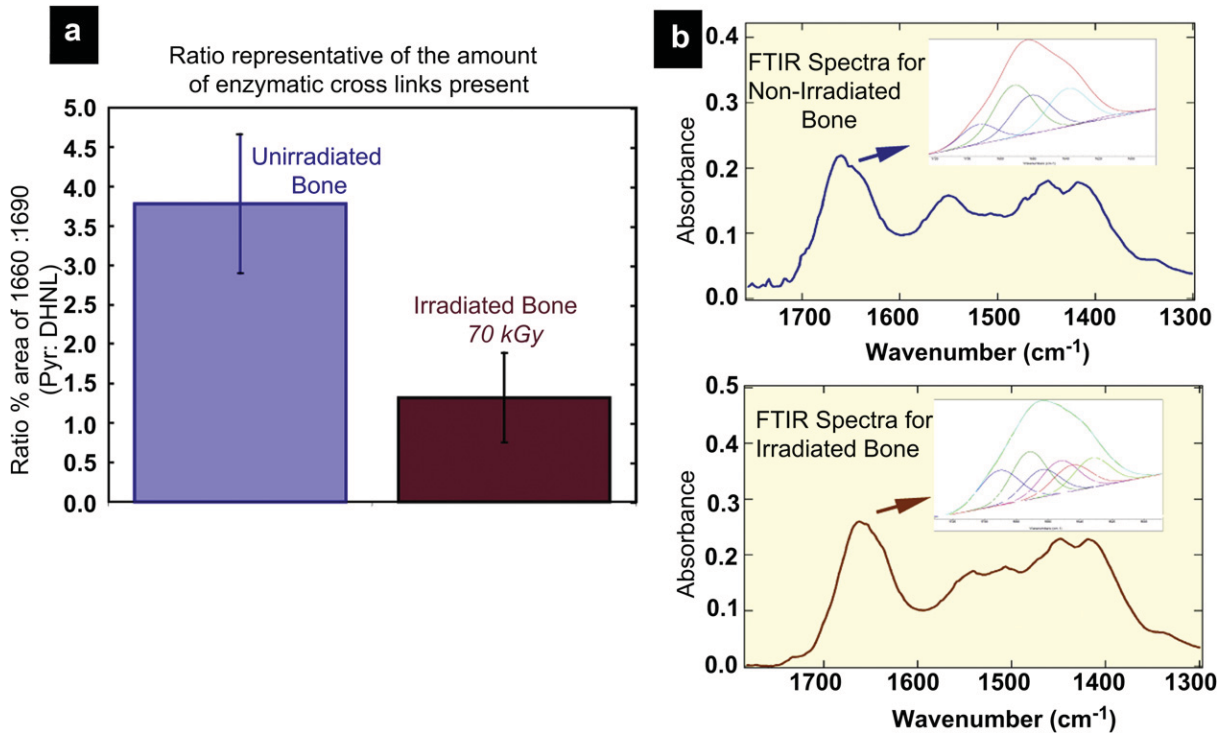

Fig. 9. Fourier transform infrared spectroscopy of human cortical bone in the unirradiated and 70 kGy irradiated condition. (a) Shows a comparison of the calculated spectroscopic ratio of the 1660:1690 cm^{-1} peaks in unirradiated and 70 kGy irradiated samples. The 1660:1690 ratios are calculated through a combination of second derivative spectroscopy to locate the position of the underlying bands within the amide I region and then peak fitting of these subbands to determine the relative percent area of each underlying component. The area 1660:1690 ratio appears to correspond to the ratio of nonreducible/reducible collagen cross-links in bone [39]. Following irradiation of 70 kGy, the 1660:1690 ratio decreases by almost a third. (b) Shows FTIR spectra and the amide I underlying bands for both groups.

to the structure of the collagen. Past studies [22,65] have used this procedure to examine the effects of gamma irradiation on the mechanical and material properties of tendon, which is primarily comprised of type I collagen organized in parallel arrays, and have reported changes to the cross-linking in collagen with increased exposure to irradiation. The collagen in both tendon and bone is stabilized by interfibrillar and intermolecular cross-links, the primary mature cross-link is hydroxypyridinium; indeed, one study demonstrated [22] a significant decrease in the hydroxypyridinium cross-link density with 60 kGy of irradiation. High doses of irradiation may also induce changes in the material properties of tendons by breaking of peptide bonds in the collagen molecules and rupture of the hydrogen bonds, although these changes occur more often in the dry, rather than wet, state.

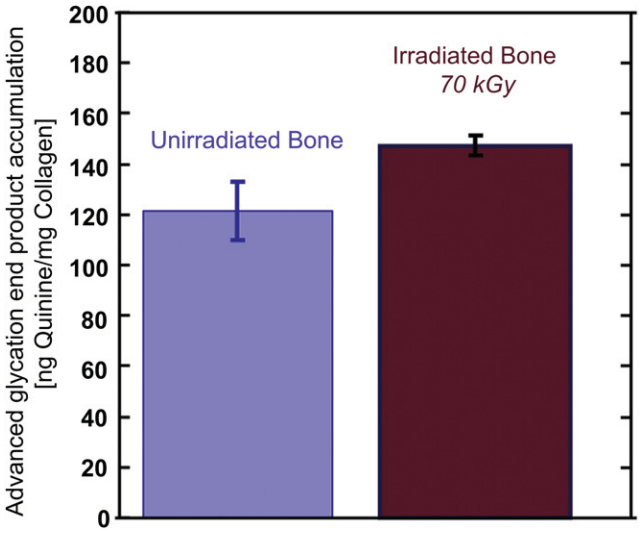

Fig. 10. The accumulation of advanced glycation end-products (AGEs) was fluorimetrically quantified in the cortex of the femora in unirradiated and 70 kGy irradiated human cortical bone samples. AGEs increase slightly when bone is irradiated with a dose of 70 kGy which increased the concentration of fluorescent (non-enzymatic) cross-links to ~21% more than in the unirradiated bone.

For the present FTIR results for unirradiated and 70 kGy irradiated bone shown in Fig. 9, the infrared spectra in the region of 1585–1720 cm^{-1} are of relevance as they show absorbance bands for the vibrations of protein amide I. Among the underlying bands that make up the amide I spectral peak, two are of particular interest, at ~1660 cm^{-1} and one at ~1690 cm^{-1}, as it has been shown that during collagen denaturing the relative intensity of the former decreases while the latter increases [39,66,67]. Indeed, the ratio of these two bands corresponds to the amount of enzymatic collagen cross-links present, specifically the non-reducible mature Pyr cross-links (interfibrillar) and the reducible immature DHNLN cross-links (intrafibrillar) found in bone [39]. In past studies, the relative areas of 1660:1690 peaks were found to increase with aging in bovine bone [39] and osteoporosis in human bone [66], while the ratio was found to decrease with vitamin B_6-deficient chicken bone [39]. We similarly find here that with 70 kGy of irradiation, the ratio of 1660:1690 peak areas decreases by almost two-thirds, indicative of major changes in cross-linking and bonding in the amide I region. With respect to the enzymatic cross-links in the collagen, the decrease in this ratio with irradiation exposure suggests that there are changes in the cross-link profile with a greater proportion of immature cross-links to the mature cross-links following irradiation [65]; indeed, either an increase in immature cross-links or a reduction in mature cross-links could disrupt the integrity of the mature cross-links, such as covalent hydroxypyridinium, leading to premature failure of the tissue.

Finally, we also find an increase in the concentration of the non-enzymatic (AGE) cross-links (Fig. 10), which are known to suppress plasticity in older bone [68,69]. Indeed, we suspect that it is these cross-links that are primarily responsible for the restriction in bone plasticity from fibrillar sliding in irradiated bone. Although the increased accumulation of AGEs in aging bone can be attributed to the longevity of the tissue and age-related changes in biological bone metabolism (including incomplete tissue remodeling and altered glucose metabolism), the mechanism of the apparent increased concentration of AGEs in irradiated bone observed is not known. It may be possible that the non-flourescent intermediate cross-links that occur during the Amadori rearrangement of sugars [40] is accelerated by irradiation, producing the fluorescent AGEs observed here. It is also important to note that the quantitative AGEs content is normalized with respect to collagen, and any loss of collagen due to the damaging irradiation could also increase the AGEs per amount of collagen. Regardless of the mechanism, however, the increase in AGEs content is consistent with the inhibition of fibrillar sliding and loss of plastic toughening observed in aging bone. These harmful effects of bone irradiation can be observed at multiple length-scales through the suppression of nano- and micro-scale plasticity mechanisms, and may be the result of alterations in the profile and distributions of the collagen cross-linking.

5. Conclusions

Based on an experimental study, spanning molecular to macroscopic length-scales, of the effects of synchrotron x-ray irradiation on the structure and mechanical properties of hydrated human cortical bone (in the transverse orientation), the following conclusions can be made:

1. Compared to healthy (unirradiated) bone, exposure to irradiation doses between 0.05 and 630 kGy progressively led to a severe degradation in strength, ductility and toughness.
2. After 630 kGy of radiation, the ultimate strength and ductility were decreased by ~80%, the work-of-fracture by ~100%, and the fracture toughness (fracture resistance) by a factor of five. No major changes in the mechanical integrity of the bone could be discerned for irradiation exposures of 35 kGy or less.
3. The irradiation-induced loss in fracture resistance is attributed to both intrinsic (plasticity) and extrinsic (shielding) contributions to the bone toughness. Compared to unirradiated bone, fracture in irradiation-damaged bone was characterized by far smaller crack-path deflections, smoother fracture surfaces, and hence much lower extrinsic toughening.
4. At irradiation doses of 70 kGy and above, stress-strain curves displayed a complete absence of post-yield plastic deformation and, with increasing irradiation, a major reduction in fracture load and toughness. The irradiation-induced suppression of bone plasticity acts to severely limit the intrinsic toughness by macroscopically embrittling the bone tissue.
5. Such irradiated-induced suppression of bone plasticity is consistent with SAXS/WAXD studies of the partitioning of strain in the bone under load, which indicated that for an applied tissue strain of ~1%, the individual strain carried by the collagen fibrils was some 40% smaller in 70 kGy irradiated bone, as compared to unirradiated bone, indicative of a lack of plasticity in the collagen.
6. The loss in intrinsic toughness through the suppression of plasticity via the mechanism of fibrillar sliding is attributed to an increased incidence of specific cross-linking of the collagen with irradiation. Measurements for unirradiated and 70 kGy irradiated bone revealed that there was a ~21% increase in the concentration of non-enzymatic cross-links, in the form of advanced glycation end-products (AGEs), in the irradiated bone, which acts to restrict fibrillar sliding of the collagen fibrils.
7. With respect to the enzymatic cross-links, we find a decreasing ratio of non-reducible (mature) to reducible (immature) cross-links in the collagen in irradiation-damaged bone. The departure from the healthy distribution of these cross-links appears to progressively disrupt the integrity of the mature cross-links, leading to lower fracture loads.
8. At very large exposure of 630 kGy, the distortion of the UV Raman spectra further suggests complete fracture of peptide bonds in the collagen backbone, which is consistent with the progressively degraded bone strength at high irradiation exposures.

Acknowledgments

This work was supported by the National Institute of Health (NIH/NIDCR) under grant no. 5R01 DE015633 to the Lawrence Berkeley National Laboratory (LBNL); support for S.Y.T. and T.A. was additionally provided by NIH grants no. R01DE019284 and F32AR059497. We acknowledge the use of the two x-ray synchrotron beam lines 7.3.3 (SAXS/WAXD) and 8.3.2 (micro-tomography) at the Advanced Light Source at the Lawrence Berkeley National Laboratory (LBNL), which is supported by the Office of Science of the U.S. Department of Energy under contract no. DE-AC02-05CH11231. The authors wish to thank Drs. Tony Tomsia, Maximilien Launey, Joel Ager, Hans Bechtel, Alex Hexemer, Andrew Tauschera, and Alastair MacDowell at LBNL for their considerable help, and Professor Tony Keaveny and Mike Jekir, of the Mechanical Engineering Department at the University of California, Berkeley, for graciously allowing us to use their facilities to machine samples for this project.

References

[1] Fratzl P, Weinkamer R. Nature's hierarchical materials. Prog Mater Sci 2007; 52:1263–334.
[2] Meyers MA, Chen PY, Lin AYM, Seki Y. Biological materials: structure and mechanical properties. Prog Mater Sci 2008;53:1–206.
[3] Rho JY, Kuhn-Spearing L, Zioupos P. Mechanical properties and the hierarchical structure of bone. Med Engin Phys 1998;20:92–102.
[4] Weiner S, Wagner HD. The material bone: structure mechanical function relations. Annu Rev Mater Sci 1998;28:271–98.
[5] Ritchie RO, Buehler MJ, Hansma PK. Plasticity and toughness in bone. Phys Today 2009;62:41–7.
[6] Launey ME, Buehler MJ, Ritchie RO. On the mechanistic origins of toughness in bone. Annu Rev Mater Res 2010;40:25–53.
[7] Ritchie RO. Mechanisms of fatigue crack propagation in metals, ceramics and composites: role of crack tip shielding. Mater Sci Eng A 1988;103:15–83.
[8] Ritchie RO. Mechanisms of fatigue-crack propagation in ductile and brittle solids. Int J Fract 1999;100:55–83.
[9] Ji B, Gao H. Mechanical properties of nanostructure of biological materials. J Mech Phys Solids 2004;52:1963–90.
[10] Gupta HS, Seto J, Wagermaier W, Zaslansky P, Boesecke P, Fratzl P. Cooperative deformation of mineral and collagen in bone at the nanoscale. Proc Natl Acad Sci 2006;103:17741–6.
[11] Koester KJ, Ager JW, Ritchie RO. The true toughness of human cortical bone measured with realistically short cracks. Nat Mater 2008;7:672–7.
[12] Koester KJ, Barth HD, Ritchie RO. Effect of aging on the transverse toughness of human cortical bone: evaluation by R-curves. J Mech Behav Biomed Mater 2011;4:1504–13.
[13] Weiner S, Traub W, Wagner HD. Lamellar bone: structure-function relations. J Struct Biol 1999;126:241–55.
[14] Wagner HD, Weiner S. On the relationship between the microstructure of bone and its mechanical stiffness. J Biomech 1992;25:1311–20.
[15] Wagermaier W, Gupta HS, Gourrier A, Paris O, Roschger P, Burghammer M, et al. Scanning texture analysis of lamellar bone using microbeam synchrotron x-ray radiation. J Appl Crystallogr 2007;40:115–20.
[16] Wasserman N, Brydges B, Searles S, Akkus O. In vivo linear microcracks of human femoral cortical bone remain parallel to osteons during aging. Bone 2008;43:856–61.

[17] Peterlik H, Roschger P, Klaushofer K, Fratzl P. From brittle to ductile fracture of bone. Nat Mater 2006;5:52–5.
[18] Vangsness CT, Garcia IA, Mills CR, Kainer MA, Roberts MR, Moore TM. Allograft transplantation in the knee: tissue regulation, procurement, processing, and sterilization. Am J Sports Med 2003;31:474–81.
[19] Cheung DT, Perelman N, Tong D, Nimni ME. The effect of gamma-irradiation on collagen molecules, isolated alpha-chains, and crosslinked native fibers. J Biomed Mater Res 1990;24:581–9.
[20] Grieb TA, Forng R-Y, Bogdansky S, Ronholdt C, Parks B, Drohan WN, et al. High-dose gamma irradiation for soft tissue allografts: high margin of safety with biomechanical integrity. J Orthop Res 2006;24:1011–8.
[21] Nguyen H, Morgan D, Forwood M. Sterilization of allograft bone: effects of gamma irradiation on allograft biology and biomechanics. Cell Tissue Banking 2007;8:93–105.
[22] Salehpour A, Butler DL, Proch FS, Schwartz HE, Feder SM, Doxey CM, et al. Dose-dependent response of gamma irradiation on mechanical properties and related biochemical composition of goat bone-patellar tendon-bone allografts. J Orthop Res 1995;13:898–906.
[23] Barth HD, Launey ME, MacDowell AA, Ager III JW, Ritchie RO. On the effect of x-ray irradiation on the deformation and fracture behavior of human cortical bone. Bone 2010;46:1475–85.
[24] Akhtar R, Daymond MR, Almer JD, Mummery PM. Elastic strains in antler trabecular bone determined by synchrotron x-ray diffraction. Acta Biomater 2008;4:1677–87.
[25] Deymier-Black AC, Almer JD, Stock SR, Haeffner DR, Dunand DC. Synchrotron x-ray diffraction study of load partitioning during elastic deformation of bovine dentin. Acta Biomater 2010;6:2172–80.
[26] Almer JD, Stock SR. Internal strains and stresses measured in cortical bone via high-energy x-ray diffraction. J Struct Biol 2005;152:14–27.
[27] Thurner PJ, Wyss P, Voide R, Stauber M, Stampanoni M, Sennhauser U, et al. Time-lapsed investigation of three-dimensional failure and damage accumulation in trabecular bone using synchrotron light. Bone 2006;39:289–99.
[28] Voide R, Schneider P, Stauber M, Wyss R, Stampanoni M, Sennhauser U, et al. Time-lapsed assessment of microcrack initiation and propagation in murine cortical bone at submicrometer resolution. Bone 2009;45:164–73.
[29] Ager III JW, Nalla RK, Breeden KL, Ritchie RO. Deep-ultraviolet Raman spectroscopy study of the effect of aging on human cortical bone. J Biomed Opt 2005;10:034012.
[30] ASTM standard E1820-09. Standard test method for measurement of fracture toughness. West Conshohocken, PA, USA: American Society for Testing and Materials; 2009.
[31] Yan JH, Mecholsky JJ, Clifton KB. How tough is bone? application of elastic-plastic fracture mechanics to bone. Bone 2007;40:479–84.
[32] Launey ME, Chen PY, McKittrick J, Ritchie RO. Mechanistic aspects of the fracture toughness of elk antler bone. Acta Biomater 2010;6:1505–14.
[33] Kinney JH, Nichols MC. X-ray tomographic microscopy using synchrotron radiation. Annu Rev Mater Sci 1992;22:121–52.
[34] Vlassenbroeck J, Dierick M, Masschaele B, Cnudde V, Van Hoorebeke L, Jacobs P. Software tools for quantification of x-ray microtomography at the 'center for x-ray tomography' at Ghent University. Nucl Instru Meth Phys Res A 2007;580:442–5.
[35] Mercury CS. Avizo™ 3D visualization framework; 2008. Chelmsford, MA.
[36] van de Weert M, van't Hof R, van der Weerd J, Heeren RMA, Posthuma G, Hennink WE, et al. Lysozyme distribution and conformation in a biodegradable polymer matrix as determined by FTIR techniques. J Control Release 2000;68:31–40.
[37] George A, Veis A. FTIRS in water demonstrates that collagen monomers undergo a conformational transition prior to thermal self-assembly in vitro. Biochem 1991;30:2372–7.
[38] Paschalis E, Mendelsohn R, Boskey A. Infrared assessment of bone quality: a review. Clin Orthop Relat Res 2011;469:2170–8.
[39] Paschalis EP, Verdelis K, Doty SB, Boskey AL, Mendelsohn R, Yamauchi M. Spectroscopic characterization of collagen cross-links in bone. J Bone Miner Res 2001;16:1821–8.
[40] Bailey AJ. Molecular mechanisms of ageing in connective tissues. Mech Ageing Dev 2001;122:735–55.
[41] Woessner JF. The determination of hydroxyproline in tissue and protein samples containing small proportions of this imino acid. Arch Biochem Biophys 1961;93:440–7.
[42] Anderson MJ, Keyak JH, Skinner HB. Compressive mechanical-properties of human cancellous bone after gamma irradiation. J Bone Jt Surg Am Vol 1992;4A:747–52.
[43] Currey JD, Foreman J, Laketic I, Mitchell J, Pegg DE, Reilly GC. Effects of ionizing radiation on the mechanical properties of human bone. J Orthop Res 1997;15:111–7.
[44] Fideler BM, Vangsness T, Lu B, Orlando C, Moore T. Gamma irradiation effects on biomechanical properties of human bone - patellar tendon - bone allografts. Am J Sports Med 1995;23:643–6.
[45] Gibbons MJ, Butler DL, Grood ES, Bylskiaustrow DI, Levy MS, Noyes FR. Effects of gamma irradiation on the initial mechanical and material properties of goat bone - patellar tendon - bone allografts. J Orthop Res 1991;9:209–18.
[46] Hamer AJ, Strachan JR, Black MM, Ibbotson CJ, Stockley I, Elson RA. Biomechanical properties of cortical allograft bone using a new method of bone strength measurement - a comparison of fresh, fresh-frozen and irradiated bone. J Bone Jt Surg Br Vol 1996;78B:363–8.
[47] Hamer AJ, Stockley I, Elson RA. Changes in allograft bone irradiated at different temperatures. J Bone Jt Surg 1999;81:342–5.
[48] Nalla RK, Kinney JH, Ritchie RO. Mechanistic fracture criteria for the failure of human cortical bone. Nat Mater 2003;2:164–8.
[49] Akkus O, Belaney RM, Das P. Free radical scavenging alleviates the biomechanical impairment of gamma radiation sterilized bone tissue. J Orthop Res 2005;23:838–45.
[50] Thompson JB, Kindt JH, Drake B, Hansma HG, Morse DE, Hansma PK. Bone indentation recovery time correlates with bond reforming time. Nature 2001;414:773–6.
[51] Fantner GE, Hassenkam T, Kindt JH, Weaver JC, Birkedal H, Pechenik L, et al. Sacrificial bonds and hidden length dissipate energy as mineralized fibrils separate during bone fracture. Nat Mater 2005;4:612–6.
[52] Krauss S, Fratzl P, Seto J, Currey JD, Estevez JA, Funari SS, et al. Inhomogeneous fibril stretching in antler starts after macroscopic yielding: indication for a nanoscale toughening mechanism. Bone 2009;44:1105–10.
[53] Gupta H, Wagermaier W, Zickler G, Hartmann J, Funari S, Roschger P, et al. Fibrillar level fracture in bone beyond the yield point. Int J Fract 2006;139:425–36.
[54] Harrington MJ, Gupta HS, Fratzl P, Waite JH. Collagen insulated from tensile damage by domains that unfold reversibly: in situ x-ray investigation of mechanical yield and damage repair in the mussel byssus. J Struct Biol 2009;67:47–54.
[55] Bailey AJ, Sims TJ, Ebbesen EN, Mansell JP, Thomsen JS, Mosekilde L. Age-related changes in the biochemical properties of human cancellous bone collagen: relationship to bone strength. Calcif Tissue Int 1999;65:203–10.
[56] Banse X, Sims TJ, Bailey AJ. Mechanical properties of adult vertebral cancellous bone: correlation with collagen intermolecular cross-links. J Bone Miner Res 2002;17:1621–8.
[57] Viguet-Carrin S, Garnero P, Delmas P. The role of collagen in bone strength. Osteoporos Int 2006;17:319–36.
[58] Wang X, Shen X, Li X, Mauli Agrawal C. Age-related changes in the collagen network and toughness of bone. Bone 2002;31:1–7.
[59] Knott L, Bailey AJ. Collagen cross-links in mineralizing tissues: a review of their chemistry, function, and clinical relevance. Bone 1998;22:181–7.
[60] Buehler MJ. Nanomechanics of collagen fibrils under varying cross-link densities: atomistic and continuum studies. J Mech Behav Biomed Mater 2008;1:59–67.
[61] Buehler MJ. Multiscale aspects of mechanical properties of biological materials. J Mech Behav Biomed Mater 2011;4:125–7.
[62] Jäger I, Fratzl P. Mineralized collagen fibrils: a mechanical model with a staggered arrangement of mineral particles. Biophys J 2000;79:1737–46.
[63] Gupta HS, Wagermaier W, Zickler GA, Raz-Ben Aroush D, Funari SS, Roschger P, et al. Nanoscale deformation mechanisms in bone. Nano Lett 2005;5:2108–11.
[64] Colwell A, Hamer A, Blumsohn A, Eastell R. To determine the effects of ultraviolet light, natural light and ionizing radiation on pyridinium cross-links in bone and urine using high-performance liquid chromatography. Eur J Clin Invest 1996;26:1107–14.
[65] Bailey AJ, Rhodes DN, Cater CW. Irradiation-induced crosslinking of collagen. Radiat Res 1964;22:606–21.
[66] Paschalis EP, Shane E, Lyritis G, Skarantavos G, Mendelsohn R, Boskey AL. Bone fragility and collagen cross-links. J Bone Miner Res 2004;19:2000–4.
[67] Saito M, Marumo K. Collagen cross-links as a determinant of bone quality: a possible explanation for bone fragility in aging, osteoporosis, and diabetes mellitus. Osteoporos Int 2010;21:195–214.
[68] Vashishth D, Gibson GJ, Khoury JI, Schaffler MB, Kimura J, Fyhrie DP. Influence of nonenzymatic glycation on biomechanical properties of cortical bone. Bone 2001;28:195–201.
[69] E A Zimmermann ES, H Bale, HD Barth, S Tang, P Reichert, B Busse, et al. Age-related changes in the plasticity and toughness of human cortical bone at multiple length-scales. Proc Natl Acad Sci; in press.